

## Rheological studies on liquid-crystal colloids prepared by dispersing spherical microparticles with homeotropic surface anchoring

Rasmita Sahoo & Surajit Dhara

To cite this article: Rasmita Sahoo & Surajit Dhara (2017) Rheological studies on liquid-crystal colloids prepared by dispersing spherical microparticles with homeotropic surface anchoring, *Liquid Crystals*, 44:10, 1582-1591, DOI: [10.1080/02678292.2017.1309469](https://doi.org/10.1080/02678292.2017.1309469)

To link to this article: <http://dx.doi.org/10.1080/02678292.2017.1309469>

 View supplementary material [↗](#)

 Published online: 30 Mar 2017.

 Submit your article to this journal [↗](#)

 Article views: 70

 View related articles [↗](#)

 View Crossmark data [↗](#)



# Rheological studies on liquid-crystal colloids prepared by dispersing spherical microparticles with homeotropic surface anchoring

Rasmita Sahoo and Surajit Dhara

School of Physics, University of Hyderabad, Hyderabad, India

## ABSTRACT

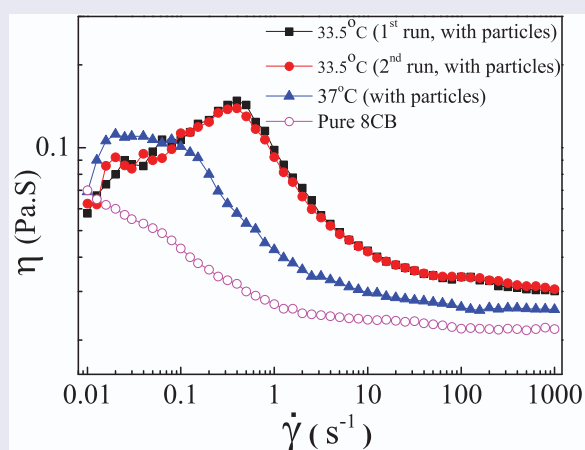
We report rheological studies on the liquid-crystal colloids prepared by dispersing silica microparticles with homeotropic surface anchoring in 8CB liquid crystal. In nematic colloids, a shear-thickening behaviour is observed in low shear rate region. The apparent yield stress of both the nematic and smectic-A (SmA) phases increases with increasing volume fraction of particles ( $\phi$ ). The critical strain amplitude ( $\gamma_c$ , i.e., crossover of  $G'$  and  $G''$ ) in SmA colloids decreases significantly with increasing  $\phi$ . The frequency-dependent storage modulus of SmA colloids show a power-law behaviour ( $G'(\omega) \sim \omega^\alpha$ ) and the loss modulus ( $G''(\omega)$ ) exhibits a shallow minimum. The optical rheomicroscopy shows that the nematic colloids form a network structure which are stretched and broken at high shear rate. When the temperature is decreased to SmA phase, the networks collapse showing regions of high-density particles. The variation of storage modulus with  $\phi$  indicates that the SmA colloids response is dominated by defects.

## ARTICLE HISTORY

Received 31 January 2017  
Accepted 10 March 2017

## KEYWORDS

Nematic colloids; smectic-A colloids; rheomicroscopy; soft glass



## 1. Introduction

The colloidal dispersion in isotropic liquids like water, oil etc. has been studied since decades due to their wide range of applications. However, the attention towards the dispersion of nano- and microparticles in anisotropic liquids like lyotropic and thermotropic liquid crystals (LCs) has created an immense interest in last two decades [1–6]. These are known as LC colloids. Usually, the nanoparticles do not create any long-range elastic distortion in the nematic liquid crystal (NLC) but the physical properties of the composites become significantly different from that of the pure LCs and such materials are potential for several

applications [7–9]. When microparticles are dispersed in nematic LCs, they induce topological defects and create elastic distortions. This results long-range forces among the particles in the medium. These forces have no analogue in common colloidal systems where particles are dispersed in the isotropic liquids. Usually, three different types of topological defects are induced by spherical microparticles in NLCs, namely, hyperbolic hedgehog, Saturn ring and boojum depending on the anchoring strength, the elastic properties of the LCs and the particle size [1,4,10,11]. There have been many interesting experimental studies reported on LC colloids. In most studies, the attention has

been paid on the topological defects induced by a variety of particles or the laser assisted self-assembly, manipulation of defects by optical tweezers [3,4,12–14].

However, a few studies have been reported on the bulk and rheological properties of LC colloids. For example, Oswald et al. studied the rheology of a lyotropic lamellar phase, where they showed under shear flow how the dislocation loops cross and connect the layers and disturb the flow [15]. Meeker et al. have found an unusual soft–solid state in 5CB (pentyl cyanobiphenyl) LC colloids prepared by dispersing PMMA (polymethylmethacrylate) nanoparticles (250 nm) [16]. Petrov et al. showed that solid cellular structures are formed in these systems [17]. Anderson et al. studied the details of the morphology of the cellular microstructures [18]. Subsequently, they studied the mechanical properties of the nematic matrix with the cellular morphology [19]. The origin of cellular structure was studied and discussed by Vollmer et al. [20,21]. Raghunathan et al. studied the elastic properties (splay and bend) of lyotropic LC colloids and found no substantial change in the elastic constants in the low particle concentrations (<2%) [22]. Poulin et al. have studied the phase separation and morphology of lyotropic colloidal systems made of small particles (60–120 nm latex polyballs) [23]. Zapotocky et al. investigated the effect of bigger silica particles (about 1  $\mu\text{m}$ ) in cholesteric LCs. From the rheological studies, they showed the effect of network of disclinations connecting the bigger clusters of particles [24]. Wood et al. dispersed nearly a micron-sized particle in 5CB and showed that the elasticity of the LC colloids increases beyond a certain concentration. They showed that it was due to the formation of percolating network structure of disclination lines. These lines are entangled with the particles giving a self-quenched defect glass state of line defects [25].

Bandyopadhyay et al. studied the rheology of LC–aerosil (7 nm) composites of smectic-A (SmA) LC (8CB) and reported a soft glassy behaviour of the composites with increasing particle density [26]. Recently, Kulkarni et al. have reported on the effect of particle loading, particle shape on the rheology and the phase-transition kinetics of lyotropic hexagonal LCs [27]. In all the above experiments, topological defects induced by the particles play a crucial role and these defects were induced mostly due to the spontaneous anchoring of the molecules on the particle's surface. In the present study, we investigate the rheological properties of LC colloids prepared by dispersing silica microparticles in 8CB LC. The particles are treated for homeotropic alignment of the LC molecules at the surface that usually induce hyperbolic

hedgehog, Saturn ring or escaped defects (bubble-gum defects) depending on the surface anchoring and confinement. We performed rheomicroscopy studies that reveal shear-dependent microstructural change of the nematic colloid that gives shear thickening. Our study suggests that with increasing volume fraction, the SmA colloids tend to emerge from soft glass to shear induced ordered state of colloids.

## 2 Experimental

In the experiment, we used monodisperse silica microspheres (average diameter 5  $\mu\text{m}$ ), coated with octadecyldimethyl (3-trimethoxysilylpropyl) ammonium chloride (DMOAP) to obtain perpendicular (homeotropic) alignment of LC molecules on the surface. Relatively larger size of the particle was chosen (than previously reported) for the purpose of simultaneous optical rheomicroscopy studies. The microspheres with different volume fractions ( $\phi$ ) namely 1–20% were dispersed in the nematic phase of 8CB LC by using a vortex mixture and ultrasonication. Rheological measurements were made by using a controlled strain rheometer (Anton Paar MCR-501). The optical rheomicroscopy setup consists of a CCD colour camera (model: Lumenera), a microscope tube and a long working-distance objective (NA = 0.4, 20 $\times$ , Nikon) [28]. A polariser and an analyser were kept crossed and placed in the tube in appropriate places. We used parallel plate geometry of diameter 43 mm provided by Anton Paar for rheomicroscopy studies. The thickness of the bottom glass plate is 6 mm. The sample was illuminated by light source through the objective from the bottom and the images were taken in the reflection mode. The microscope tube is adjustable in both the horizontal and vertical directions for the focusing purpose. The gap maintained between two parallel glass plates was 0.075 mm. The temperature of the sample was controlled by a Peltier temperature controller. The compound 4-cyano-4'-octylbiphenyl (8CB) was obtained from Sigma-Aldrich and exhibits the following phase sequence: I 39.7 $^{\circ}\text{C}$  N 32.4 $^{\circ}\text{C}$  SmA. These temperatures are measured by the Peltier temperature controller of the rheometer. All the experiments were performed in cooling the sample from the nematic to SmA phase.

## 3. Results and discussion

### 3.1. Nematic colloids

First, we observed the textures and the phase-transition temperatures of sample using polarising optical

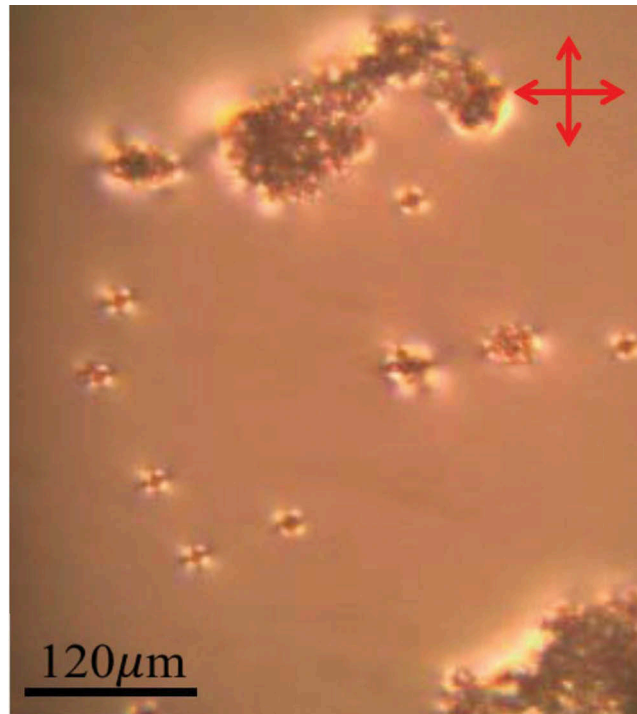


**Figure 1.** Rheomicroscopy image taken under crossed without shear for  $\phi = 1\%$  in the nematic phase ( $35^\circ\text{C}$ ). Four bright lobes showing the director distortion due to the Saturn ring defects associated with the particles.

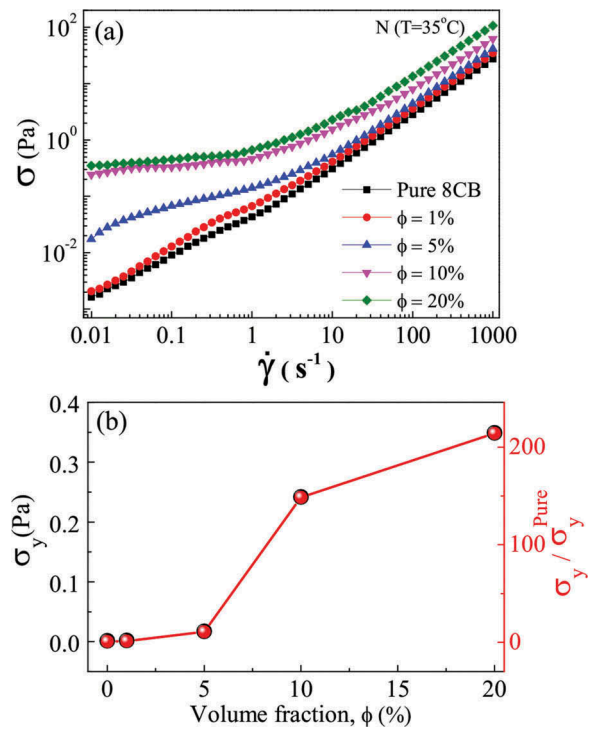


**Figure 2.** (a) Shear rate-dependent shear stress ( $\sigma$ ) and (b) yield stress ( $\sigma_y$ ) at various volume fractions at a fixed temperature ( $T = 35^\circ\text{C}$ ).

microscope. There was no appreciable change in the nematic–isotropic and nematic–SmA phase-transition temperatures. This was further confirmed by differential scanning calorimetry studies (see Supplementary Information) [29]. The sample was mounted on the rheometer's plate in the nematic phase.

Figure 1 shows the texture observed under rheomicroscope after mounting (without shear). Most of the particles are agglomerated in smaller domains and only a few of them are dispersed individually. The isolated particles in Figure 1 show four visible-coloured lobes of director distortion suggesting they have quadrupolar director configuration [25].

The sample was presheared at a low shear rate ( $\dot{\gamma} = 10 \text{ s}^{-1}$ ) for 5 min before starting the measurements. Figure 2(a) shows the shear rate-dependent shear stress at different concentrations of particles in the nematic phase ( $35^\circ\text{C}$ ). The apparent yield stress ( $\sigma_y$ ) is increasing with increasing volume fraction of particles. Above shear rate  $10 \text{ s}^{-1}$ , the stress is proportional to the shear rate and this behaviour is typical for nematics at high shear rate. Figure 2(b) shows the variation of yield stress ( $\sigma_y$ ) as a function of volume fraction ( $\phi$ ). Up to  $\phi = 5\%$ , it shows a small but linear increase and beyond this  $\sigma_y$  changes slope and increases rapidly. For example,  $\sigma_y$  at  $\phi = 20\%$  is approximately 200 times larger than that of the pure 8CB (Figure 2(b)). The linear increase of stress is expected in dilute colloidal systems (Einstein's relation). The rapid increase in the  $\sigma_y$  suggests that there are some collective response of the particles.

To get more insight into the dilute systems, we looked at the textures in the rheomicroscope and measured the shear rate dependent viscosity at various temperatures. The sample was presheared at a high shear rate ( $\dot{\gamma} = 500 \text{ s}^{-1}$ ) for 5 min to disperse the particles.

Figure 3 shows the variation of apparent viscosity at  $\phi = 1\%$  in the nematic phase at various temperatures. A clear shear-thickening behaviour is observed in the nematic phase (with particles) at all temperatures in the low shear rate range. This behaviour is significantly different than the shear-thinning behaviour of nematic without particles (open circles in Figure 3).

Figure 4 shows some representative images taken at different shear rates at temperature  $33.5^\circ\text{C}$  for  $\phi = 1\%$ . With increasing shear rate, different microstructures of the particles are observed. In the low shear rate range ( $0.01\text{--}0.4 \text{ s}^{-1}$ ), the colloidal chains are bridged to form a network structure. The increase of the yield stress (Figure 2(b)) with volume fraction of particles is due to these network structures. In the shear-thickening region, the network is stretched, accompanied by deformation of the bridging chains. Increasing the shear rate increases the stress on the network structures and once the critical force is exceeded (about  $\dot{\gamma} = 0.6 \text{ s}^{-1}$ ), they begin to break into smaller chains showing a shear-thinning behaviour. The shear thinning continues as long as the breaking process continues. At higher shear rate ( $\dot{\gamma} = 39.8 \text{ s}^{-1}$ ), the chains start to break and forms relatively shorter chains. This shear-thickening mechanism is somewhat similar to those reported in micelle forming associating polymers in water [30]. At much higher shear rate  $\dot{\gamma} = 100 \text{ s}^{-1}$ , many chains tend to align normal to the shear direction. At the same time, many long disinclination lines are appeared (Figure 4,  $\dot{\gamma} = 100\text{--}150 \text{ s}^{-1}$ ). These line defects could be similar to those observed in microchannels by Sengupta *et al.*[31]. With increasing shear, the nematic director is orientated more uniformly and the nearly perpendicular orientation of the chains is consistent with the quadrupolar defect structure. In particular, in aligned cells, the quadrupolar chains

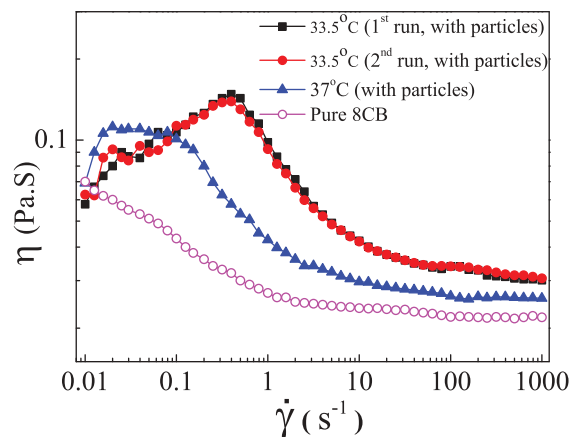
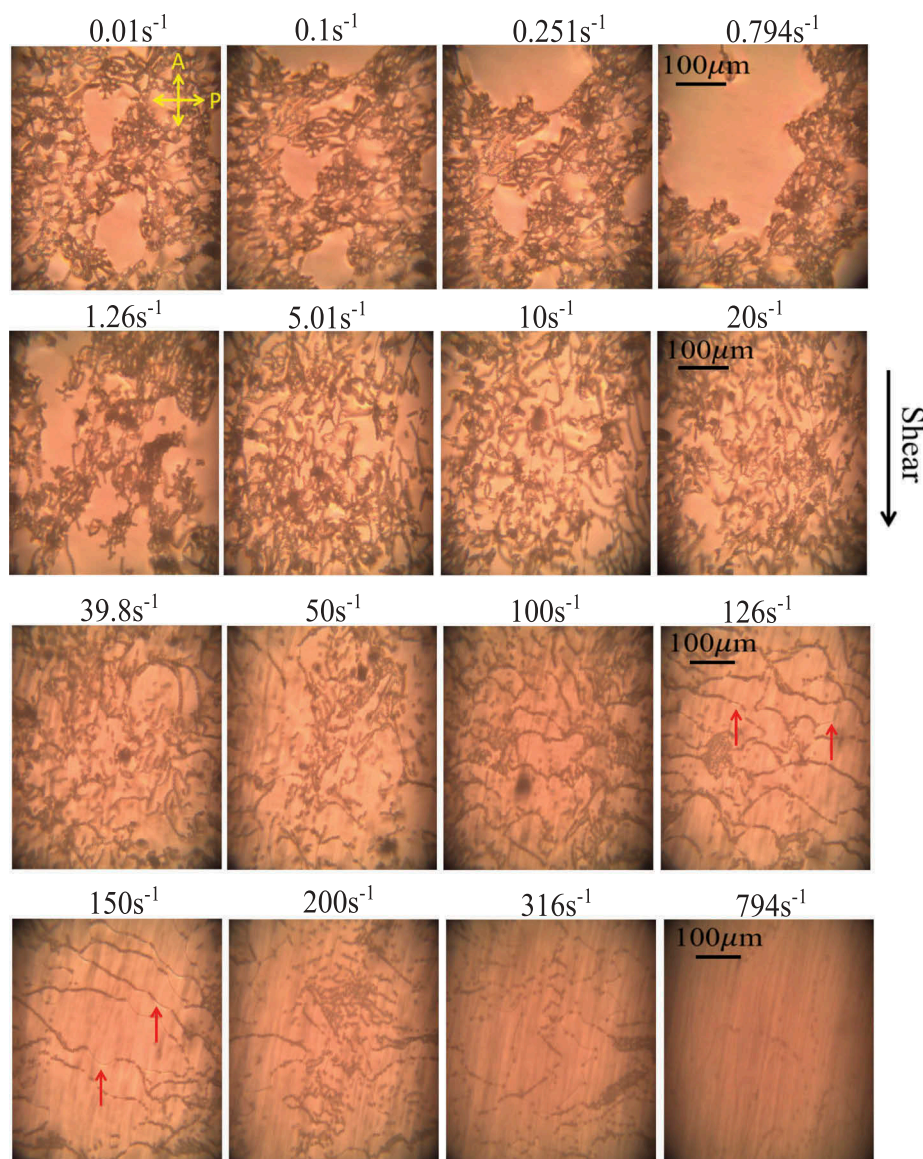


Figure 3. (Colour online) Variation of apparent viscosity  $\eta$  at a few temperatures at concentration  $\phi = 1\%$ .



**Figure 4.** (Colour online) Representative rheomicroscopy images taken during the measurement of shear rate-dependent shear viscosity in the nematic phase at  $33.5^\circ\text{C}$  for  $\phi = 1\%$ . Red arrows indicate the disclination lines.

tend to align perpendicular to the nematic director. At very high shear rate (above  $\dot{\gamma} = 200 \text{ s}^{-1}$ ), the short chains further break into individual particles which are connected by the disclination lines. This can be understood based on the competing effect of shear energy and elastic interaction energy of the particles. The approximate shear energy of a particle can be written as  $E = 6\pi\eta\dot{\gamma}ha^2$ , where  $\eta$  is the apparent viscosity,  $h$  is the gap between the plates and  $a$  is the radius of the particles. The estimated shear energy at  $\dot{\gamma} = 20 \text{ s}^{-1}$  is about  $10^6 k_B T$ . Typical elastic interaction energy per particle is about a few thousand  $k_B T$  [4]. However, this energy is expected to be a few orders of magnitude larger in the network (because a large

number of particles are involved) and comparable to the shear energy. When the shear energy exceeds the elastic interaction energy, the breaking of chains into individual particles is expected.

### 3.2. *SmA colloids*

Induced defects and colloidal interaction in SmA LCs are not well understood so far. There are a few studies on the transformation of the topological defects across the nematic–SmA phase transition [12–14] in uniformly aligned cells. The induced disorder by the foreign particles in the SmA phase is expected to affect the mechanical properties. Hence, we carried out

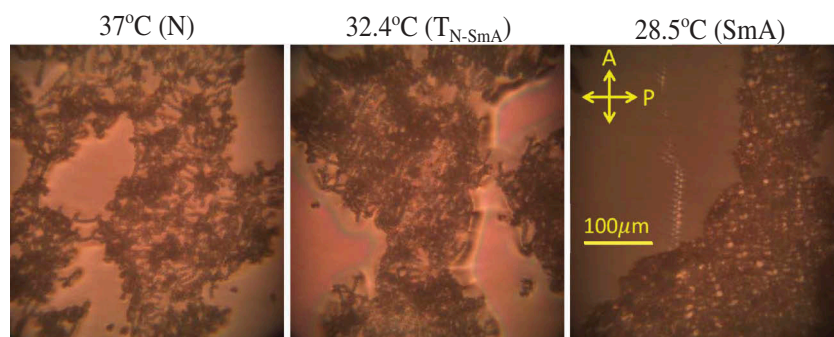


**Figure 5.** (Colour online) Some representative rheomicroscopy images taken across the N–SmA phase transition (shear rate  $\dot{\gamma} = 1 \text{ s}^{-1}$ ).

rheological measurements in the SmA phase. **Figure 5** shows some representative rheomicroscopy images taken across the N–SmA phase transition. We observed that as the SmA phase is approached, the networks tend to get compressed and in the SmA phase, the particles are collapsed creating focal conic texture. The regions without particles are well aligned (no focal conic texture). Unlike the nematic phase, no colloidal chains are observed in the SmA phase. Isolated colloidal particles with quadrupolar defect across the N–SmA phase transition have been studied by us in planar-aligned cell [14]. The Saturn ring disappears at the transition and there is a boundary

condition violation at the interface, and clear layer structure around the particles cannot be directly deduced from the optical micrographs [14].

**Figure 6(a)** shows the variation of shear stress in the SmA phase (28°C) at various volume fractions. The apparent yield stress ( $\sigma_y$ ) increases with increasing volume fraction of particles. For example,  $\sigma_y$  for pure SmA is about 0.33 Pa and it increases to 51 Pa at  $\phi = 20\%$ ; hence, this is about 150 times larger (**Figure 6(b)**).

**Figure 7** shows the variation of storage ( $G'$ ) and loss ( $G''$ ) moduli, as a function of applied strain  $\gamma$  at different volume fractions. Two important observations are made

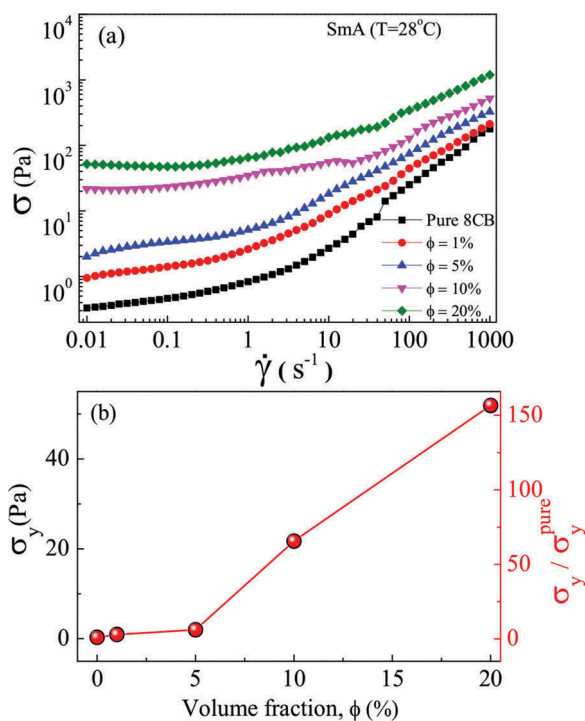


**Figure 6.** (Colour online) (a) Shear rate-dependent shear stress in the SmA phase (28°C) at various volume fractions of particles. (b) Variation of yield stress ( $\sigma_y$ ) with  $\phi$  obtained from **Figure 6(a)**.

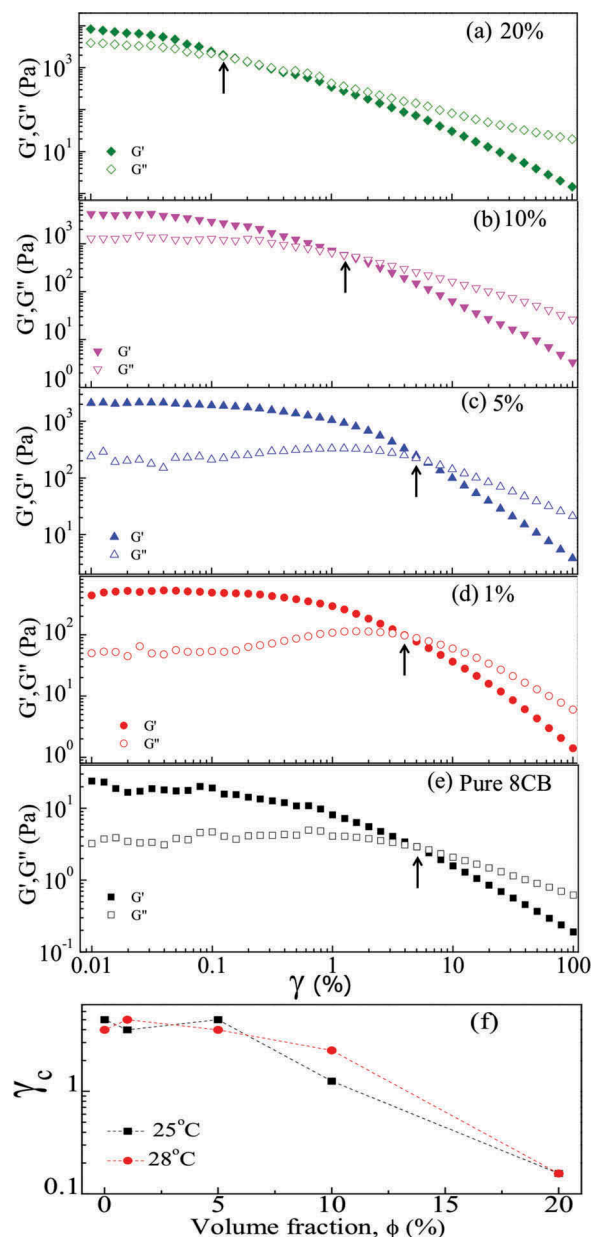


**Figure 7.** (Colour online) (a)–(e) Strain dependence of the storage  $G'$  and loss  $G''$  moduli with increasing volume fraction of particle at constant angular frequency  $\omega = 1$  rad/s at  $T = 25^\circ\text{C}$ . The arrows indicate the crossover. (f) The variation of critical strain amplitude,  $\gamma_c$  (the crossover of  $G'$  and  $G''$ ), at different volume fractions.

[1]; both the elastic moduli ( $G'$  and  $G''$ ) increase and [2] the critical strain amplitude  $\gamma_c$  (crossover of  $G'$  and  $G''$ ) decreases with increasing  $\phi$ . For example,  $G'$  is 300 times larger in LC composite with  $\phi = 20\%$  compared to the pure 8CB. The variation of  $\gamma_c$  (strain induced yielding) with  $\phi$  at two different temperatures is shown in Figure 7 (f). It is observed that  $\gamma_c$  is decreasing with increasing  $\phi$ . For example, the value of  $\gamma_c$  for 0–10% is one order of magnitude larger than that of  $\phi = 20\%$ . This behaviour can be explained based on the jammed domains of

particles as seen in the rheomicroscopy (Figure 5, Sma phase). With increasing  $\phi$ , the number density and size of these jammed domains increase. As they are fragile, under low strain amplitude, they can break and flow; as a result, the critical strain amplitude ( $\gamma_c$ ) is expected to decrease [32].

It is known that the colloidal suspension can undergo glass transition with increasing particle concentration and can crystallise under favourable

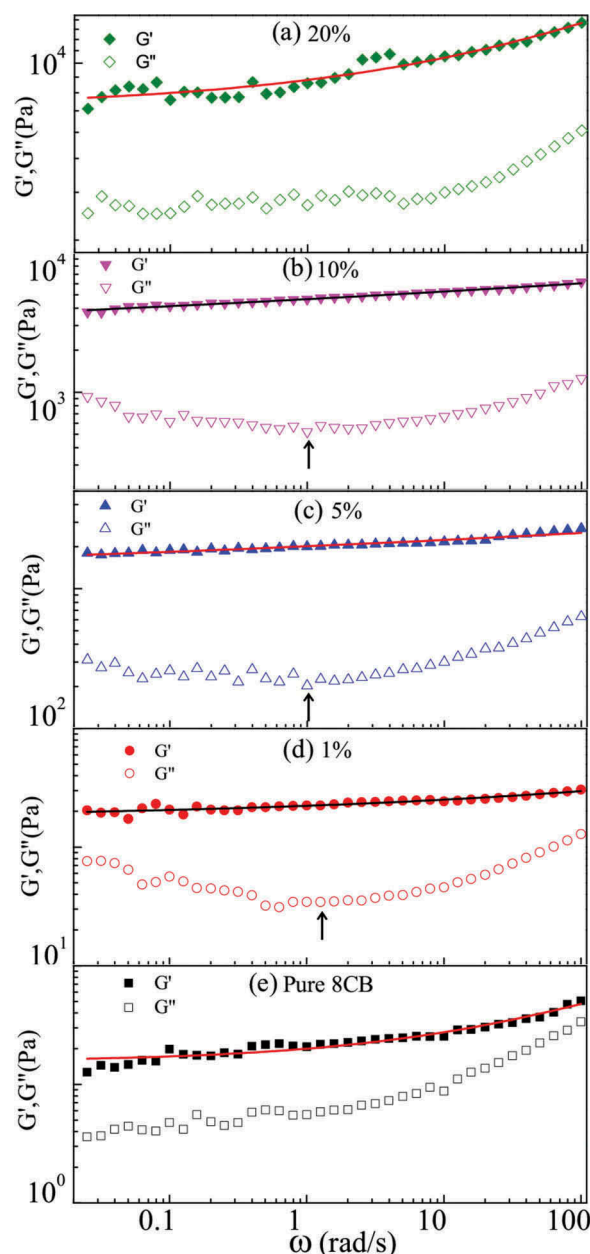


**Figure 8.** (Colour online) Angular frequency dependence of storage ( $G'$ ) and loss ( $G''$ ) moduli at different volume fractions at constant strain amplitude 0.03% at  $T = 25^\circ\text{C}$ . Continuous lines are the best fit to Equation (1). Vertical arrows indicate the minimum in  $G''$ .

condition [32,33]. To see this aspect, we studied the frequency dependence of the storage ( $G'$ ) and loss ( $G''$ ) moduli. Figure 8 shows the angular frequency dependence of  $G'$  and  $G''$  at different volume fractions.

The SmA phase (without colloids) shows typical frequency dependence, i.e. both moduli are increasing with frequency. It is noted that for  $\phi = 1\%$ ,  $5\%$  and  $10\%$ ,  $G''(\omega)$  exhibits a shallow minimum. This is due to the increase in  $G''(\omega)$  at both lower and at higher frequencies. The low frequency rise is due to a very slow structural rearrangement of the particles suggesting that there exists a relaxation process. The high-frequency rise signifies the

domination of viscous relaxation of fluid phase [34,35]. This is also a typical characteristic of many colloidal soft glasses. Hence, we analyse the results based on the soft glassy rheology model. In this model, the real part of the storage modulus is given by Refs [36,37]:

$$G'(\omega) = G_0 + \beta\omega^\alpha \quad (1)$$

where  $G_0$  is the plateau modulus that arises due to the static defects in SmA and the frequency-dependent term results from the bulk response of the materials.  $\beta$  arises from the disorientated (misaligned) parts of the sample [26,36,38]. The fit parameters are plotted with volume

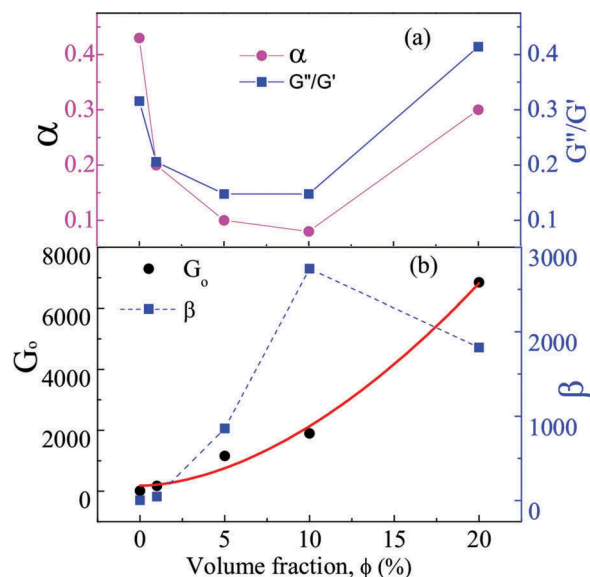


**Figure 9.** (Colour online) (a) Variation of  $\alpha$  and the ratio  $G''/G'$  as a function of volume fraction of particles  $\phi$ . (b) Variation of  $G_0$  and  $\beta$  with  $\phi$ . The red line is the best fit result  $G_0 \sim \phi^{1.8 \pm 0.2}$ .

fraction in Figure 9. It is observed that  $\alpha$  decreases with increasing volume fraction and tends to zero ( $\alpha \rightarrow 0$ ) up to  $\phi = 10\%$  (Figure 9(a)). Similar behaviour was also observed in many colloidal soft glassy materials [26,33]. The variation of the ratio  $G''/G'$  with  $\phi$  is also shown in Figure 9(a). We observe that  $G''/G' \sim \alpha$  as expected in the soft glassy rheology model [26,37,39]. Figure 9(b) shows the variation of  $G_0$  and  $\beta$  with volume fraction. The increase of  $\beta$  with  $\phi$  indicates that the contribution from the disoriented parts of the sample increases due to the inclusion of the particles. The increase of  $G_0$  indicates that the smectic line defects dominate this soft glassy rheology. Theoretically in analogy with rubber elasticity, the elastic response of static defect networks should vary as  $G_0 \sim \rho^2$ , where  $\rho$  is the density of the particles [26,36]. In our experiment, we find that  $G_0 \sim \phi^{1.8 \pm 0.2}$  (Figure 9(b)). Similar exponent was also reported in case of aerosil-dispersed SmA LCs (8CB) [26]. At higher concentrations ( $\phi = 20\%$ ), both  $\alpha$  and the ratio  $G''/G'$  tend to increase with  $\phi$ . We conjecture that at this high-volume fraction of particles under oscillation, some short-range order among the particles is developed. However, further study is required.

#### 4. Conclusion

In conclusion, we have studied the rheological properties of nematic and SmA LC colloids prepared by dispersing spherical microparticles with homeotropic boundary condition in 8CB LCs. The microparticles create chains

mediated by the induced defects with quadrupolar director configuration and form networks with increasing volume fraction. We observed a shear-thickening behaviour in the low shear rate range. The rheomicroscopy studies reveal the shear rate-dependent distinct dynamics of the networks. The dynamic response of the SmA colloids shows a soft glassy rheology with increasing volume fractions up to a certain range. Finally, this study shows that the rheological properties of nematic and SmA colloids are significantly contributed by the particle-induced defects and their self-assembly.

#### Acknowledgements

We gratefully acknowledge the support from UPE-II, DST (Project ref.: DST/SJF/PSA-02/2014-2015), CSIR (Project ref.: 03(1207)/12/EMR-II). R.S. acknowledges UGC for BSR fellowship.

#### Disclosure statement

No potential conflict of interest was reported by the authors.

#### Funding

We gratefully acknowledge the support from UPE-II, DST (Project ref.: DST/SJF/PSA-02/2014-2015), CSIR (Project ref.: 03(1207)/12/EMR-II). R.S. acknowledges UGC for BSR fellowship.

## References

- [1] Stark H. Physics of colloidal dispersions in nematic liquid crystals. *Phys Rep.* **2001**;351:387–474.
- [2] Poulin P, Stark H, Lubensky TC, et al. Novel colloidal interactions in anisotropic fluids. *Science.* **1997**;275:1770–1773.
- [3] Smalyukh II, Lavrentovich OD, Kuzmin AN, et al. Elasticity-mediated self-organization and colloidal interactions of solid spheres with tangential anchoring in a nematic liquid crystal. *Phys Rev Lett.* **2005**;95:157801.
- [4] Musevic I, Skarabot M, Tkalec U, et al. Two-dimensional nematic colloidal crystals self-assembled by topological defects. *Science.* **2006**;313:954–958.
- [5] Serra F. Curvature and defects in nematic liquid crystals. *Liq Cryst.* **2016**;43:1920–1936.
- [6] Nemitz IR, Eleney KM, Crudden CM, et al. Chiral periodic mesoporous organosilica in a smectic-A liquid crystal: source of the electrooptic response. *Liq Cryst.* **2016**;43:497–504.
- [7] Garbovskiy Y. Electrical properties of liquid crystal nano-colloids analysed from perspectives of the ionic purity of nano-dopants. *Liq Cryst.* **2016**;43:648–653.
- [8] Basu R, Garvey A. Effects of ferroelectric nanoparticles on ion transport in a liquid crystal. *Appl Phys Lett.* **2014**;105:151905.
- [9] Sahoo R, Rasna MV, Lisjak D, et al. Magnetodielectric and magnetoviscosity response of a ferromagnetic liquid crystal at low magnetic fields. *Appl Phys Lett.* **2015**;106:161905.
- [10] Chernyshuk SB, Tovkach OM. Colloidal particles as elastic triads in nematic liquid crystals. *Liq Cryst.* **2016**;43:2410–2421.
- [11] Kim SJ, Lee BK, Kims JH. Inter-particle interactions of weak homeotropic anchoring with electric field in a homogeneous nematic cell. *Liq Cryst.* **2016**;43:1589–1596.
- [12] Zuhail KP, Sathyanarayana P, Sec D, et al. Topological defect transformation and structural transition of two-dimensional colloidal crystals across the nematic to smectic-A phase transition. *Phys Rev E(R).* **2015**;91:030501.
- [13] Zuhail KP, Dhara S. Temperature dependence of equilibrium separation and lattice parameters of nematic boojum-colloids. *Appl Phys Lett.* **2015**;106:211901.
- [14] Zuhail KP, Copar S, Musevic I, et al. Spherical micro-particles with Saturn ring defects and their self-assembly across the nematic to smectic-A phase transition. *Phys Rev E.* **2015**;92:052501.
- [15] Oswald P, Allain M. Rheology and structural defects in a lyotropic lamellar phase. *J Colloid Interface Sci.* **1988**;126:45–53.
- [16] Meeker SP, Poon WCK, Crain J, et al. Colloid-liquid-crystal composites: an unusual soft solid. *Phys Rev E(R).* **2000**;61:R6083–R6086.
- [17] Petrov PG, Terentjev EM. Formation of cellular solid in liquid crystal colloids. *Langmuir.* **2001**;17:2942–2949.
- [18] Anderson VJ, Terentjev EM, Meeker SP, et al. Cellular solid behaviour of liquid crystal colloids 1. Phase separation and morphology. *Eur Phys J E.* **2001**;4:11–20.
- [19] Anderson VJ, Terentjev EM. Cellular solid behaviour of liquid crystal colloids 2. Mechanical properties. *Eur Phys J E.* **2001**;4:21–28.
- [20] Vollmer D, Hinze G, Poon WCK, et al. The origin of network formation in colloid-liquid crystal composites. *J Phys.: Condens Matter.* **2004**;16:L227–L233.
- [21] Vollmer D, Hinze G, Ullrich B, et al. Formation of self-supporting reversible cellular networks in suspensions of colloids and liquid crystals. *Langmuir.* **2005**;21:4921–4930.
- [22] Raghunathan VA, Richetti P, Roux D. Dispersion of latex particles in a nematic solution. *Langmuir.* **1996**;12:3789–3792.
- [23] Poulin P, Raghunathan VA, Richetti P, et al. On the dispersion of latex particles in a nematic solution. I. Experimental evidence and a simple model. *J Phys II France.* **1994**;4:1557–1569.
- [24] Zapotocky M, Ramos L, Poulin P, et al. Particle-stabilized defect gel in cholesteric liquid crystals. *Science.* **1999**;283:209–212.
- [25] Wood TA, Lintuvuori JS, Schofield AB, et al. A self-quenched defect glass in a colloid-nematic liquid crystal composite. *Science.* **2011**;334:79–83.
- [26] Bandyopadhyay R, Liang D, Colby RH, et al. Enhanced elasticity and soft glassy rheology of a smectic in a random porous environment. *Phys Rev Lett.* **2005**;94:107801.
- [27] Kulkarni S, Thareja P. Rheology of colloidal particles in lyotropic hexagonal liquid crystals: the role of particle loading, shape, and phase transition kinetics. *Rheol Acta.* **2016**;55:23–36.
- [28] Sahoo R, Chojnowska O, Dabrowski R, et al. Experimental studies on the rheology of cubic blue phases. *Soft Matter.* **2016**;12:1324–1329.
- [29] Supplementary information contains DSC data.
- [30] Yekta A, Xu B, Duhamel J, et al. Fluorescence Studies of associating polymers in water: determination of the chain end aggregation number and a model for the association process. *Macromolecules.* **1995**;28:956–966.
- [31] Sengupta A, Tkalec U, Bahr C. Nematic textures in microfluidic environment. *Soft Matter.* **2011**;7:6542–6549.
- [32] Koumakis N, Schofield AB, Petekidis G. Effects of shear induced crystallization on the rheology and ageing of hard sphere glasses. *Soft Matter.* **2008**;4:2008–2018.
- [33] Chen DTN, Wen Q, Janmey PA, et al. Rheology of soft materials. *Annu Rev Condens Matter Phys.* **2010**;1:301–322.
- [34] Mason TG, Weitz DA. Linear viscoelasticity of colloidal hard sphere suspensions near the glass transition. *Phys Rev Lett.* **1995**;75:2770–2773.
- [35] Mason TG, Bibette J, Weitz DA. Elasticity of compressed emulsions. *Phys Rev Lett.* **1995**;75:2051–2054.
- [36] Ramos L, Zapotocky M, Lubensky TC, et al. Rheology of defect networks in cholesteric liquid crystals. *Phys Rev E.* **2002**;66:031711.
- [37] Sollich P, Lequeux F, H braud P, et al. Rheology of soft glassy materials. *Phys Rev Lett.* **1997**;78:2020–2023.
- [38] Sahoo R, Ananthaiah JA, Dabrowski R, et al. Rheology of twist-grain-boundary-A liquid crystals. *Phys Rev E.* **2014**;90:012506.
- [39] Nair GG, Krishna Prasad S, Bhargavi R, et al. Soft glass rheology in liquid crystalline gels formed by a mono-disperse dipeptide. *J Phys Chem B.* **2010**;114:697–704.